ASSOCIATED CONTENT

Figure S1**. Surface defects of different types:**

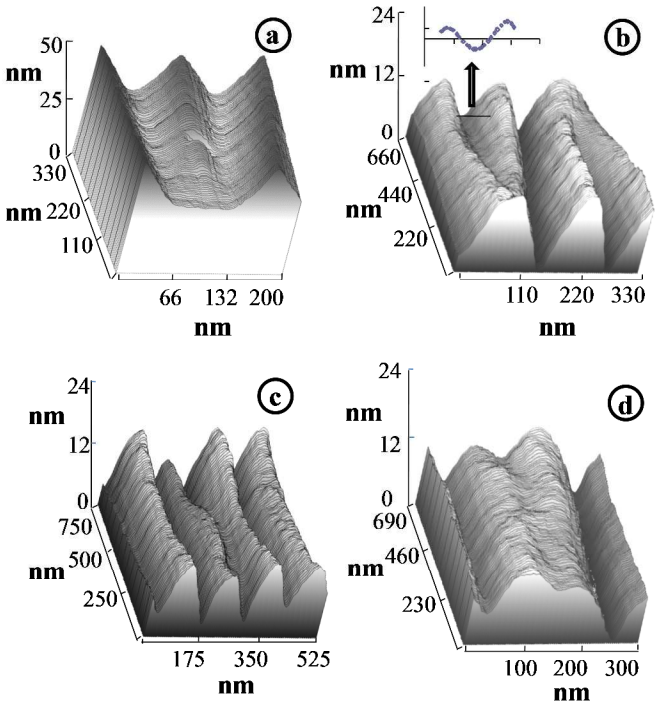

Figure S1. Images (f) and (g) represent the single and double kink type defect formed on 1st generation wrinkles and the images (h – i) represent the other type of defects formed on 2nd generation wrinkles: (h) slip and (i) sandwich. (j) Plot of radius of curvature as a function of extension ratio for 1st and 2nd generation wrinkles respectively.

Beside the peak curvatures and the distribution of their occurrence, the other features of the wrinkled surfaces are the defects as shown in Supplementary Fig. 1. In essence, the defects are the locations, where, the cylindrical folds, being not parallel along their length, eventually merge forming the kinks. Increase in extension ratio of the PDMS film results in increase in the density of defects which form into different types in the 2nd generation patterns. Images (a) and (b) show a defect on $S_1|_{40\%}$ surface, images (c) and (d) represent the ones on kinks of different types on $S_2|_{40\%}$ surfaces. These 2nd generation kinks are of different types: double kink, slip kink and sandwiched kink respectively.

Figure S2. Effect of protein concentration on crystallization on nano-wrinkled surfaces

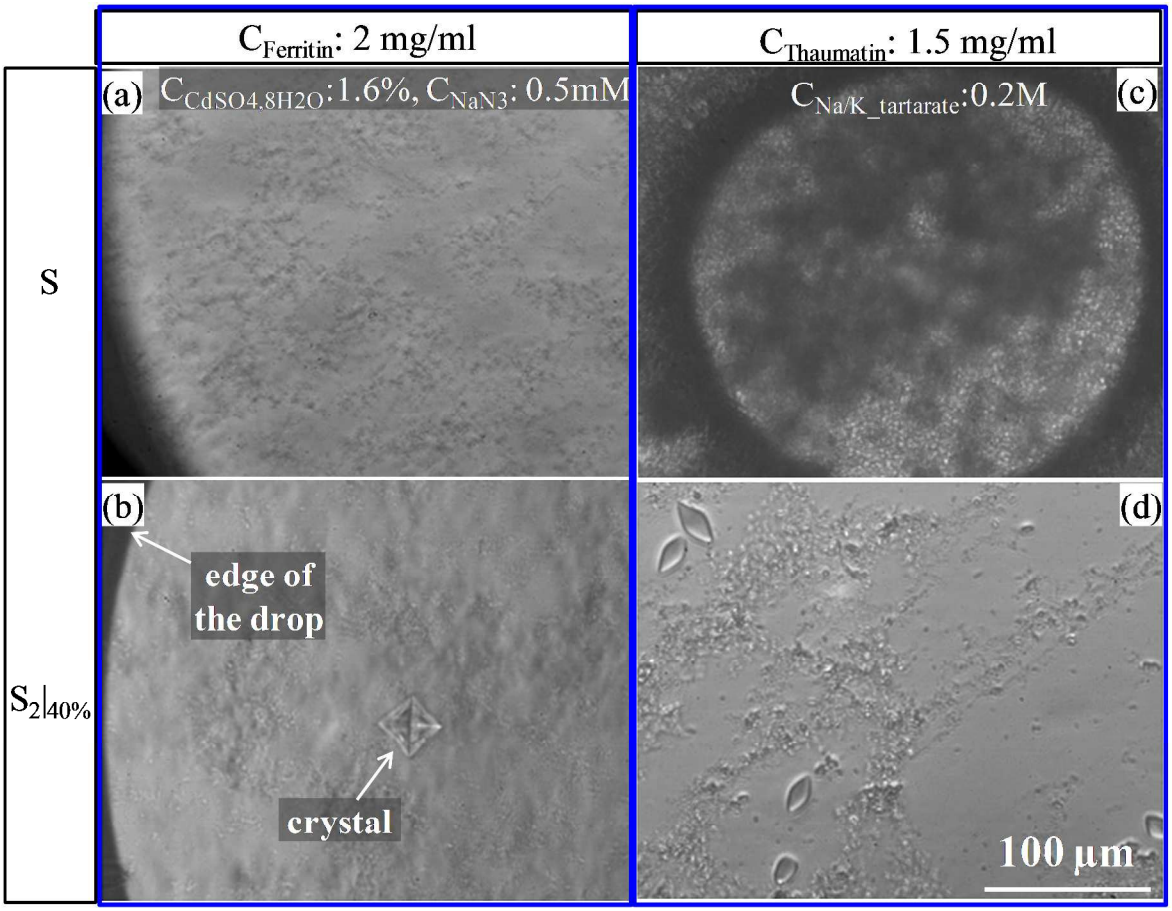

Figure S2. The concentration of protein in buffer was varied keeping that of the precipitant unaltered. (a and b) Optical micrographs show that at small enough concentration of ferritin, e.g. at 2 mg/ml, and with no ammonium sulfate, $C_{ammonium\_sulfate}$ = 0, whereas no crystal appears on the control surface S, small crystals appear on the $S_2|_{40\%}$ surface, not at the drying front of the sandwiched drop, but towards its center. (c, d) Similarly, for very small concentration of thaumatin ~1.5mg/ml, no crystal is observed on the S surface, however, crystals nucleated on the $S_2|_{40\%}$ surface.

Figure S3. X-ray diffraction analysis of Ferritin and Glucose isomerase crystals

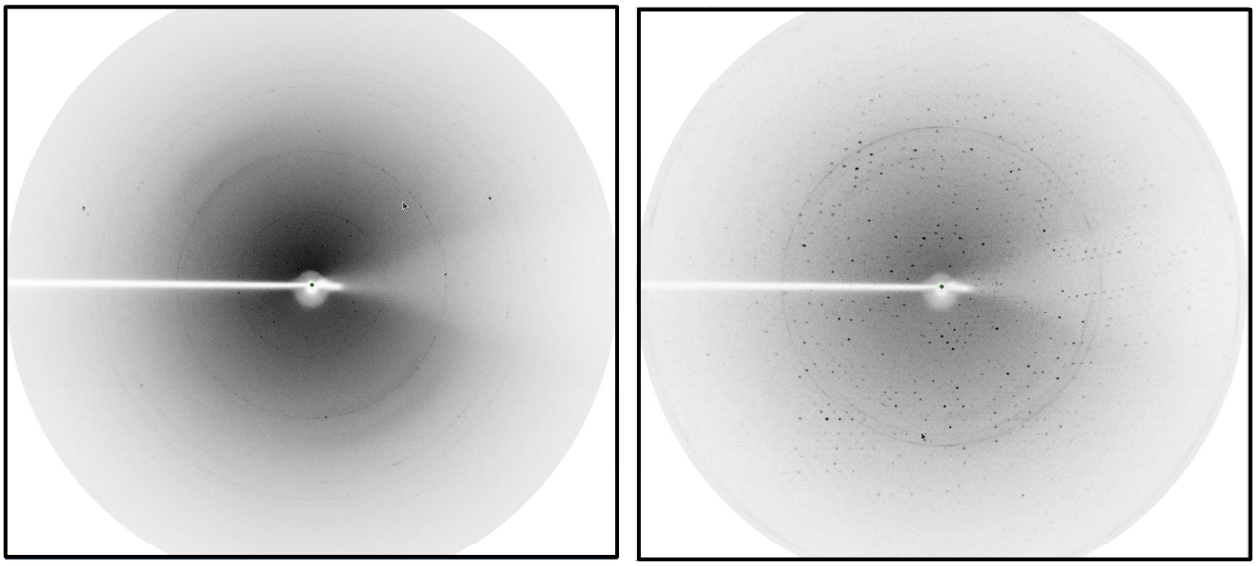

a **b**

Figure S3. X-ray diffraction pattern of Ferritin (a) and Glucose Isomerase (b) crystals.

Figure S4. Crystallization of Xylanase II on different surfaces using Calcium chloride as the precipitant

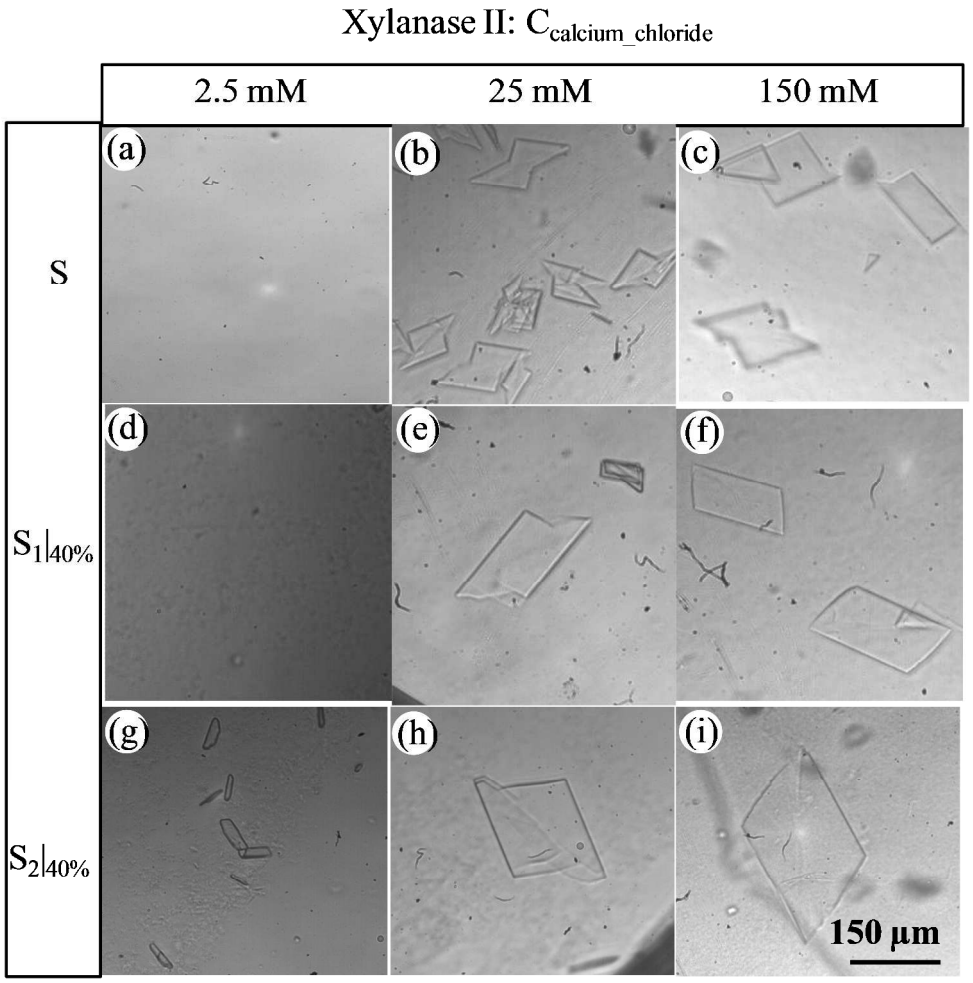

Figure S4. The optical micrographs depict thin plate shaped crystals of Xylanase II grown on three different substrates: S, $S_1|_{40\%}$ and $S_2|_{40\%}$ by varying the concentration of the precipitant, i.e. calcium chloride, $C_{calcium\_chloride}$= 2.5 to 150 mM. On the control surface S, crystals do not appear for small precipitant concentration, $C_{calcium\_chloride}$ = 2.5 mM, at higher concentration of the precipitant, small crystals appear in an uncontrolled manner, in large numbers. In contrast, on the $S_2|_{40\%}$ surface, nucleation occurs even at very small concentration of the precipitant; at higher concentrations, few large crystals appear signifying controlled nucleation.

Figure S5. Crystal size as a function of precipitant concentration as obtained on different surfaces

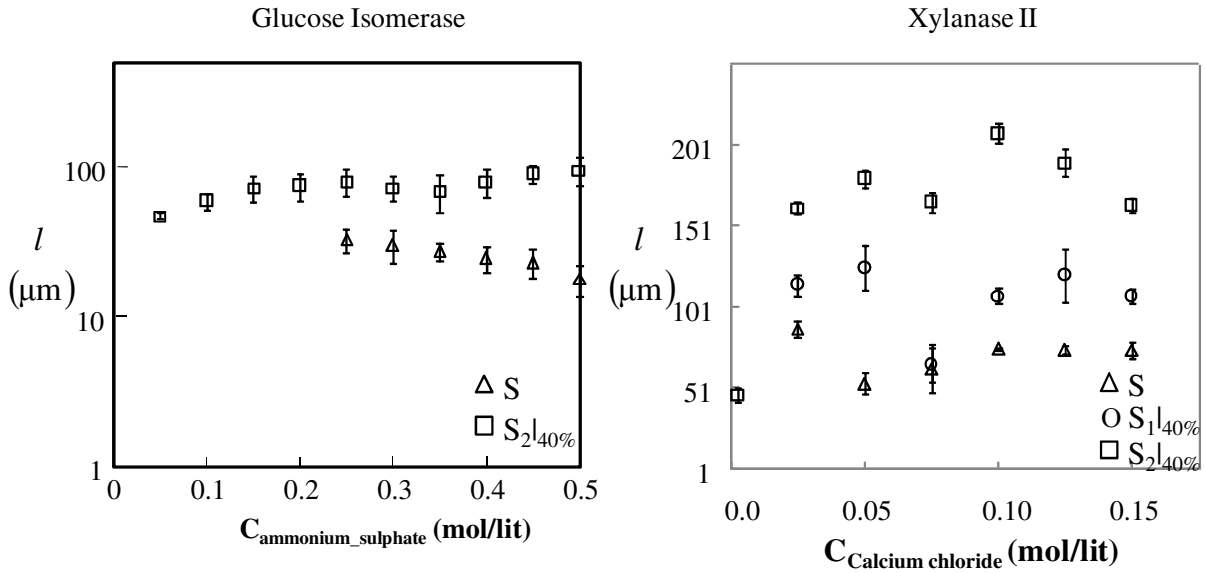

Figure S5. The plots of crystal size *l* vs $C_{ammonium\_sulphate}$ and *l* vs $C_{calcium\_chloride}$ depict the distribution of crystal sizes over a wide range of precipitant concentrations for glucose isomerase (a) and xylanase II at three different substrates S, $S_1|_{40\%}$ and $S_2|_{40\%}$.

Figure S6. Plate shaped Xylanase II crystal after the dye test